CZECH TECHNICAL UNIVERSITY
IN PRAGUE

Faculty of Nuclear Sciences and Physical
Engineering

Department of Physics

RESEARCH THESIS

CHARACTERIZATION OF SILICON PARTICLE DETECTOR PROPERTIES

Bc. Markéta Sedláčková

Supervisor: Ing. Mária Čarná

Prague, 2013

Prohlášení:

Prohlašuji, že jsem výzkumný úkol vypracovala samostatně a použila jsem pouze podklady (literaturu, software, atd.) uvedené v přiloženém seznamu.

Nemám závažný důvod proti užití tohoto školního díla ve smyslu 60 Zákona .121/2000 Sb., o právu autorském, o právech souvisejících s právem autorským a o změně některých zákonů (autorský zákon).

V Praze dne

Title:
Characterization of Silicon Particle Detector Properties

Author: Markéta Sedláčková

Specialization: Experimental nuclear and particle physics

Sort of project: Research work

Supervisor: Ing. Mária Čarná

Abstract: Introduction to interaction of particles with matter, radiation damage, semiconductors and pixel detectors are given in this work. Medipix2 and Timepix detectors are described in more depth. Results of measurement performed with Medipix2 detector concerning radiation hardness are presented. The degradation study of Medipix2 chip was studied. It was shown that with increasing irradiation time, the number of hits in the sensor and active pixels diminished. Also, after annealing, the default analog current value of the irradiated Medipix2 chip increased for 0.1 A.

Key words: Radiation hardness, Medipix, Pixel detector

Název práce:
Charakterizace křemíkových vlastností detektorů

Autor: Markéta Sedláčková

Abstrakt: Tento výzkumný úkol obsahuje úvod do interakce ionizujícího záření s hmotou, radiačního poškození, polovodičů a pixelových detektorů. Detektory Medipix2 a Timepix jsou více představeny v samostatné kapitole. Výsledky měření provedeného s detektorem Medipix2 jsou prezentovány. V tomto měření bylo sledování radiační poškození čipu Medipix2. Zjistilo se, že s rostoucím časem ozařování čipu, klesal počet naměřených zásahů a počet měřících pixelů v senzoru. Dále bylo zjištěno, že po měření byla zvýšena spotřeba analogového proudu o 0.1 A.

Klíčová slova: Radiační odolnost, Medipix, Pixelový detektor

Acknowledgement

I would like to express my great gratitude to my supervisor Mária Čarná for her professional feedback and help during my work. I would like to thank also to Michal Marčišovský and Martin Hejtmánek who have provided me with more feedback suggestions concerning both this work and data analysis.

Contents

Introduction **1**

1 Interaction of particles with matter **2**
1.1 Passage of particles . . . 2
1.1.1 Heavy charged particles . . . 2
1.1.2 Electrons . . . 4
1.1.3 Photons . . . 5
1.1.4 Neutrons . . . 7
1.2 Dosimetric variables . . . 8

2 Semiconductor detectors **10**
2.1 Semiconductor materials . . . 10
2.1.1 Types of semiconductors . . . 11
2.1.2 The p-n junction . . . 12
2.2 Types of semiconductor detectors . . . 12
2.3 Pixel Detectors . . . 14
2.3.1 Processing . . . 15
2.3.2 Pixels at ATLAS detector . . . 16

3 Medipix **20**
3.1 Medipix2 . . . 20
3.2 Timepix . . . 21
3.3 Readout systems . . . 22

4 Radiation hardness **24**
4.1 Displacement damage . . . 24
4.2 Ionization damage . . . 25
4.3 Radiation damage in silicon detectors . . . 25

5 Results **26**
5.1 Irradiation setup . . . 26
5.2 Measurement results . . . 27

Conclusions **32**

Bibliography **34**

Introduction

Silicon pixel detector is a type of a semiconductor detector that is nowadays widely used in high energy physics. Also, some steps are being taken to distribute this technology into other fields. The aim of this research work is therefore to provide an introduction to this part of physics.

The first chapter concerns with the description of different ways the particles interact with matter covering the most common types of particles. At the end of this chapter is written a small introductio to dosimetry.

The aim of this research work is to introduce the reader to the world of semiconductor detectors and, when the basics are presented, introduce Medipix detector.

The introduction to semiconductor detectors takes place in Chapter 2. Basic principles, not-so-basic information and some running semiconductor experiments are listed here. Types of position sensitive detectors is listed and among them the pixel detectors processing and their use is described.

Next chapter is dedicated to the Medipix, pixel detector used in the analysis presented in Chapter 5. The topic of the analysis was study radiation hardness. This phenomenon is introduced in Chapter 4.

1 Interaction of particles with matter

This chapter is divided into two parts. The first will cover the basics of particle passage through matter and the second part will be an introduction to dosimetry.

1.1 Passage of particles

To study the passage of particles through matter it is useful to study the mechanisms first. It is convenient to divide all particles into following groups:

- Heavy charged particles
- Electrons
- Neutrons
- X-rays and gamma rays

The first two are *charged* which makes their identification easier – they constantly interact with the surrounding environment through coulombic force. The other two, *uncharged*, need first to be made to interact somehow in the environment and once this is achieved they can be identified later through secondary particles, heavy charged particles in the case of neutrons and electrons in the case of photons. All these four groups interact with the surrounding medium in a different way, which is why this classification is widely used.

Every group of particles can be also characterized by the typical distance traveled by the ionizing particle in the surrounding medium. For heavy charged particles it is of order 10^{-5} m and 10^{-3} m for the electrons. As emphasized above, without interaction the uncharged particles pass through the medium unobserved, however in case of an interaction their characteristic distance traveled is of order 10^{-1} m for both types. The difference between X-rays and gamma rays is in their wavelength.

1.1.1 Heavy charged particles

Amongst heavy charged particles belong: proton, deuteron, alpha particle, or particles of high energy such as muons or kaons.

These particles interact with their surroundings and lose their energy through four different processes:

- Excitation and ionization of atoms

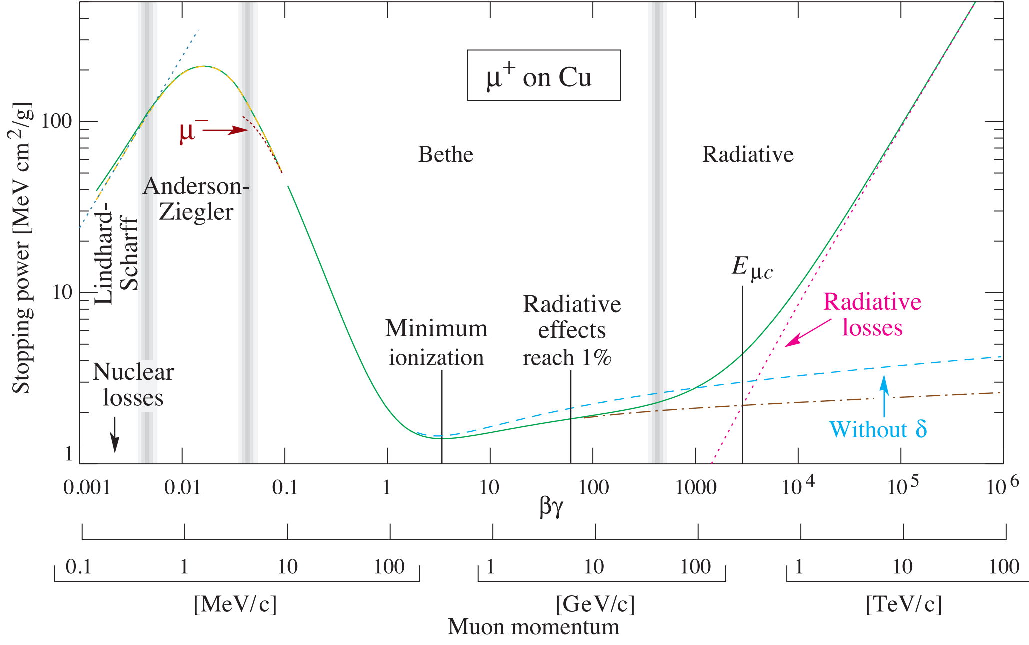

Figure 1.1: Stopping power ($= -dE/dx$) for positive muons in copper as a function of $\beta\gamma = p/Mc$ over nine orders of magnitude in momentum (12 orders of magnitude in kinetic energy). [2]

- Polarization of atoms (high energy)
- Electron capture
- Elastic scattering

The particle eventually stops or decays in the medium. The *linear stopping power* S for charged particles is defined as:

$$S = -\frac{dE}{dx},$$

where the value of $-dE/dx$ along a particle track is also called the *specific energy loss*. The classical expression used to describe specific energy loss is called the Bethe formula and is written as [1]:

$$-\frac{dE}{dx} = \left(\frac{e^2}{4\pi\epsilon_0}\right)^2 \frac{4\pi z^2 n_e}{m_e v^2} \left[\ln \frac{2m_e v^2}{I(1-\beta^2)} - \beta^2\right], \tag{1.1}$$

where v and ze are the velocity and charge of the primary particle, n_e is the electron density of the absorber, m_e is the electron rest mass, e is the electronic charge, ϵ_0 is the vacuum permitivity and I is the mean excitation potential of the target. The experimental formula for the mean excitation potential is $I = 13.5Z$, where Z is the atomic number of the absorber. β is used to denote a fraction v/c, where c is the speed of light.

In Fig. 1.1, the stopping power of a positive muon in copper is plotted. Solid line indicates the total stopping power. It is convenient to divide the curve into several sections that display different properties. In the momentum range from 0 to 1 MeV/c the Bethe formula is not valid, because the charge exchange between the particle and the absorber, which is not described by this formula, becomes important. In the next section (1 MeV/c to 1 GeV/c), the Bethe formula 1.1 can be approximated as: $-dE/dx \approx 1/v^2 \approx 1/E$; the ionization loss increases as the particle velocity

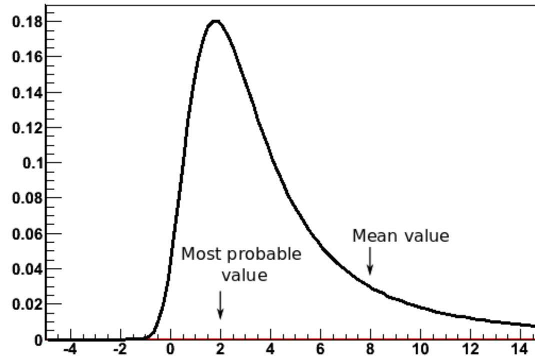

Figure 1.2: Landau distribution with most probable values shown

decreases. The end of this section is an area of minimum ionization. Particles within its energetic range are often called MIPs = Minimum Ionizing Particles and they are very hard to detect. Before the radiative effects start taking place (in the range from 1 to 10 GeV/c), the Bethe formula can be approximated as: $-dE/dx \approx \ln E$.

Landau distribution

One thing to be noted is that the detection of particles follows a statistical fluctuation denoted by a Landau distribution. This means that when a particle of a given energy enters the detector, the energy deposited (and read out) ranges from the average value given by the Bethe formula (see Eq. 1.1). The outcome of the statistical fluctuations can be seen in Fig. 1.2. This figure also shows the commonly acknowledged peaks of probabilities of such a distribution.

The probability density for value x in a Landau distribution is proportional to [3]:

$$p(x) = \int_0^{\infty} \sin 2t \exp -t\frac{x-\mu}{\sigma} - \frac{2}{\pi} t \log t \mathrm{d}t, \tag{1.2}$$

where μ is the location parameter and σ is the scale parameter. In Fig. 1.2 is shifted by $\mu = 2$ and scaled by $\sigma = 1$.

Bragg curve

The Bragg curve, which is shown in Fig. 1.3 describes the stopping power as a function of the material depth. As can be seen from the figure the stopping power increases until it quickly drops back to zero. This phenomenon is called the Bragg peak and is of importance in radiation therapy.

1.1.2 Electrons

Electrons passing through matter lose their energy through two different processes:

- Ionization and excitation of atomic electrons
- Radiation of a photon – bremsstrahlung

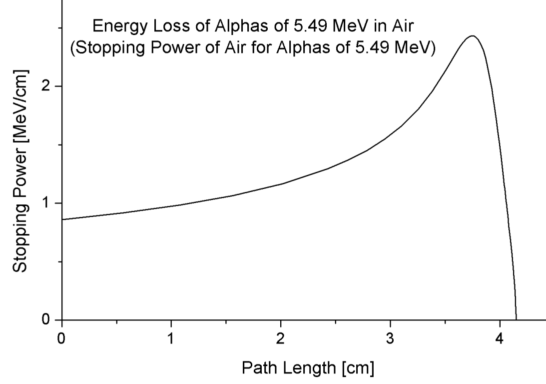

Figure 1.3: The Bragg curve of 5.49 MeV alphas in air. [4]

The first case is described by the modified Bethe formula [1]:

$$\begin{aligned} -\left(\frac{dE}{dx}\right)_{ion} &= \left(\frac{e^2}{4\pi\epsilon_0}\right)^2 \frac{2\pi n_e}{m_e v^2} \times \\ \times &\left[\ln\frac{m_e v^2 T}{2I^2(1-\beta^2)} - (\ln 2)\left(2\sqrt{1-\beta^2} - 1 + \beta^2\right) + (1-\beta^2) + \frac{1}{8}\left(1-\sqrt{1-\beta^2}\right)^2\right], \end{aligned} \tag{1.3}$$

where the symbols have the same meaning as in Eq. 1.1. These are the collisional losses. However, electrons may also lose their energy through radiative processes. They appear in the form of bremsstrahlung – an electromagnetic radiation produced by the electron deceleration when deflected by another charged particle, such as nucleus. The linear specific energy loss for radiative processes is:

$$-\left(\frac{dE}{dx}\right)_{rad} = \frac{NEZ(Z+1)e^4}{137 m_e^2 c^4}\left(4\ln\frac{2E}{m_e c^2} - \frac{4}{3}\right), \tag{1.4}$$

The dependence can be also written as: $dE/dx \sim Z^2/m^3$ which indicates that these losses are only significant in absorber materials with high atomic number. The ratio of the specific energy losses is given by:

$$\frac{(dE/dx)_{rad}}{(dE/dx)_{ion}} \cong \frac{EZ}{700}, \tag{1.5}$$

The total linear stopping power is the sum of the two types of losses:

$$\frac{dE}{dx} = \left(\frac{dE}{dx}\right)_{ion} + \left(\frac{dE}{dx}\right)_{rad}. \tag{1.6}$$

1.1.3 Photons

There are three most important interaction mechanisms of gamma rays with matter. The mechanisms are listed below as follows ordered with increasing energy of the incoming photon.

- Photoelectric absorption
- Compton scattering

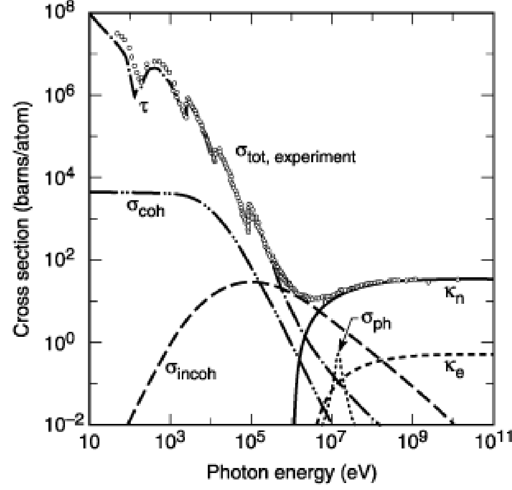

Figure 1.4: Total photon cross section σ_{tot} in lead, as a function of energy. [5]

- Electron-Positron (e^-e^+) pair production

This fact can be better seen in Fig. 1.4 displaying the total photon cross section as a function of energy, where σ_{coh} stands for the Rayleigh scattering, σ_{incoh} is the Compton scattering, κ_n is the pair production in nuclear field, κ_e is the pair production in electric field and σ_{ph} is the photonuclear absorption.

In photoelectric absorption, a photon interacts with an absorber atom in a way that the photon is absorbed and a new photoelectron appears. The photoelectron appears with an energy given by $E_e = E_\gamma - E_b$, where E_γ is the energy of incoming photon and E_b is the binding energy of the photoelectron in its atomic shell. The probability of this process is $\approx Z^4/E_\gamma^{3.5}$.

Compton scattering (schematics shown in Fig. 1.5) is a process where an incoming photon of energy E_γ hits an electron at rest, which is then recoiled and the photon is scattered into different direction through an angle θ with respect to its original direction and different energy E'_γ, summing the equation as $e + \gamma \to e + \gamma$. The energy of the scattered photon is given by:

$$E'_\gamma = \frac{E_\gamma}{1 + \frac{E_\gamma}{m_e c^2}(1 - \cos\theta)}. \tag{1.7}$$

The probability of Compton scattering is $\approx Z/E_\gamma$. Another type of photon interaction with matter is Rayleigh scattering, which is a coherent scattering, i.e. neither the photon nor electron change their energy and only their directions change. An analogy of Compton scattering called inverse Compton scattering exists for electrons. It involves the scattering of low energy photons to high energies by ultrarelativistic electrons so that the photons gain and the electrons lose energy. The process is called inverse because the electrons lose energy rather than the photons, the opposite of the standard Compton effect.

The pair production ($\gamma \to e^- + e^+$) can happen only if E_γ is higher than the rest mass of the two electrons (i.e. 1.02 MeV). However, the cross section of this interaction is small for E_γ around 1 MeV, but it becomes predominant for the many-MeV photons. During this process a photon interacts with a nucleus and a pair of electron and positron is created provided that there is enough energy available to create the pair and that both energy and momentum are conserved. Also, this interaction has to happen in the coulomb field of a nucleus so that the momentum of the process is conserved.

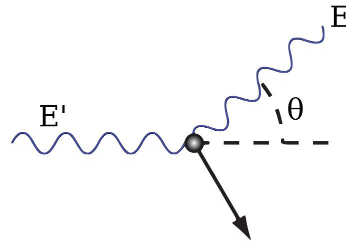

Figure 1.5: Compton scattering. [4]

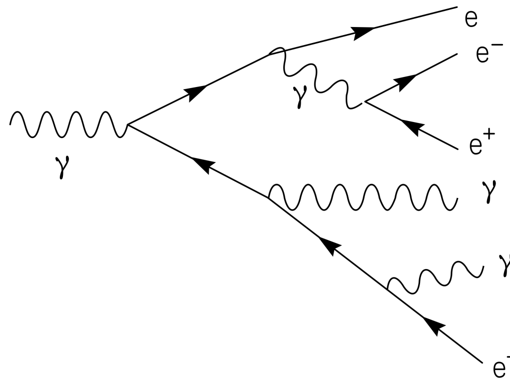

Figure 1.6: Electromagnetic particle shower. [4]

Electromagnetic shower

Electromagnetic shower (for schematic view see Fig. 1.6) starts when an electron or photon enters an absorber material. High energy photons primarily interact through pair creation, i.e. high energy electron and positron are created. These two then interact through radiating a photon (bremsstrahlung). the cycle continues until the energy of photons is lower than energy needed for pair production or until the pairs are completely stopped in the material.

This property of photons and electrons is used in high energy physics (denoted HEP) to determine the incoming energy of particle. Many modern high energy experiments contain an *electromagnetic calorimeter*, whose main property is to induce these showers.

1.1.4 Neutrons

Neutrons are uncharged particles, whose main reactions with the surrounding matter are elastic scattering and above 1.8 MeV also nuclear reactions. The secondary particles coming from neutrons are in most cases the heavy charged particles.

Therefore, two types of detectors are used for neutron detection: reaction-type and recoil-type. The information about neutron's energy is lost in both types. Reaction-type detectors are based

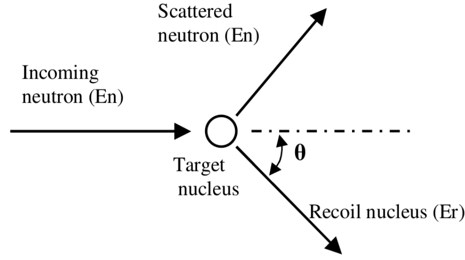

Figure 1.7: Neutron scattering kinematics. [4]

on (n,α) or (n,γ) nuclear reactions. The three most common reactions used are:

$$n + {}^{3}He \rightarrow {}^{3}H + {}^{1}H + 0.764 \text{ MeV} \tag{1.8}$$

$$n + {}^{6}Li \rightarrow {}^{4}He + {}^{3}H + 4.79 \text{ MeV} \tag{1.9}$$

$$n + {}^{10}B \rightarrow {}^{7}Li^{*} + {}^{4}He \rightarrow {}^{7}Li + {}^{4}He + 0.48 \text{ MeV } \gamma + 2.3 \text{ MeV} \quad (94\%) \tag{1.10}$$

$$\rightarrow {}^{7}Li + {}^{4}He + 2.8 \text{ MeV} \quad (6\%) \tag{1.11}$$

Neutron detector is therefore coated with conversion material ($\approx 1\mu$m thin) that starts the reaction. Recoil-type detectors use elastic scattering: incoming neutron scatters the target nucleus and through the scattering angle an energy deposited per reaction can be determined. Energy of the reaction is given as:

$$E_R = \frac{2A}{(1+A)^2}\,(1-\cos\theta)\,E_N, \tag{1.12}$$

where A is the mass number of the target nucleus and the other variables are explained in Fig. 1.7.

1.2 Dosimetric variables

Ionizing radiation has an effect on human body which varies with type and energy of radiation. The study of such effects is called dosimetry. It introduces new variables used to quantise these effects and some common variables used are listed below.

KERMA

This abbreviation stands for Kinetic Energy Released per unit Mass. It is defined as:

$$K = \frac{\mathrm{d}E_{tr}}{\mathrm{d}m}, \tag{1.13}$$

where $\mathrm{d}E_{tr}$ is the sum of the initial kinetic energies of all charged particles liberated by uncharged particles in a mass $\mathrm{d}m$. The medium should always be specified. There are various primary standards to realize K for various particle types and energies. The unit is J$\cdot$kg^{-1}; however, the special name for the unit of kerma is Gray (Gy).

Absorbed dose

This variable is defined as:

$$D = \frac{\mathrm{d}\bar{\varepsilon}}{\mathrm{d}m}, \tag{1.14}$$

where $\mathrm{d}\bar{\varepsilon}$ is the mean energy imparted to matter of mass $\mathrm{d}m$. The energy imparted is the sum of all the energy entering the volume minus all the energy leaving the volume, and incorporates

Type and energy of radiation R	w_R
Photons, all energies	1
Electrons and muons, all energies	1
Neutrons	
< 10 keV	5
10 to 100 keV	10
> 0.1 to 2 MeV	20
> 2 to 20 MeV	10
> 20 MeV	5
Protons > 2 MeV	5
Alpha particles, fission fragments, heavy nuclei	20

Tissue or organ	w_T
Gonads	0.20
Bone marrow	0.12
Colon	0.12
Lung	0.12
Stomach	0.12
Bladder	0.05
Breast	0.05
Liver	0.05
Oesophagus	0.05
Thyroid	0.05
Skin	0.01
Bone surface	0.01
Remainder	0.05
Whole body total	1.00

Table 1.1: Examples of the radiation weighting factor w_R (left) and the tissue weighting factor w_T (right). [6]

any mass energy conversions, e.g. pair production inside the volume will decrease the energy in the volume by 1.022 MeV. The medium should always be specified, since there are again various primary standards to account for various particle types and energies. The unit is J$\cdot$kg^{-1} and again the special name Gray (Gy) us used.

Equivalent dose

Equivalent dose H_T is defined as:

$$H_T = \sum_R w_R D_{T,R}, \tag{1.15}$$

where w_R is the radiation weighting factor and $D_{T,R}$ is the absorbed dose (averaged over a tissue or organ T) due to radiation of type R. $D_{T,R}$ cannot be measured experimentally. The weighting factor w_R is introduced to weight the absorbed dose for biological effectiveness of the particles (examples are shown in Table 1.1). The unit is J$\cdot$kg^{-1}; the special name for the unit of equivalent dose used is Sievert (Sv).

Effective dose

Effective dose is again represented in Sievert (Sv) unit and it is defined as:

$$H = \sum_T w_T H_T = \sum_T w_T \sum_R w_R D_{T,R}, \tag{1.16}$$

where w_R is the radiation weighting factor, $D_{T,R}$ is the absorbed dose defined above and w_T is a tissue weighting factor which reflects the total detriment to health. An example of the values of the weighting factor can be found in Table 1.1.

2 Semiconductor detectors

2.1 Semiconductor materials

Materials can be divided into three groups: conductors, semiconductors and insulators. The difference between these three types is in the distance of their valence and conductive band. [1] For insulators, the width is around 6 eV, i.e. there is minimal chance for electrons to pass from the valence band and become conductive. In conductors these bands overlap. Last but not least, the gap size in semiconductors is approximately 1 eV, which means that very few electrons gain enough thermal energy to leap the band gap at the room temperature, but their electrical properties can be controlled via other ways.

The focus of this work will be on silicon semiconductor detectors, especially pixels, therefore the list of silicon properties is shown in Table 2.1.

Even at thermal energy some electron-hole pairs are created. The probability per unit time of this generation is given by:

$$p(T) = CT^{3/2} \exp\left(-\frac{E_g}{2kT}\right), \tag{2.1}$$

where T is the absolute energy, E_g is the bandgap energy, k is the Boltzmann constant and C is the proportionality constant characteristic to the material. Once created, both the electron and the hole start to move away from their point of origin randomly. This movement is called diffusion. The distribution of the floating charges in time is a broadening Gaussian function with a standard deviation given by $\sigma = \sqrt{2Dt}$, where D is the diffusion coefficient and t is the elapsed time. The diffusion coefficient can be described as:

$$D = \mu \frac{kT}{e}, \tag{2.2}$$

where μ is the mobility of the charge carrier, k is the Boltzmann constant, T is the absolute energy and e is the charge of an electron. At 20°C the numerical value of kT/e is 0.0253 V. [1]

When an external field is applied to the semiconductor material, both the electron and the hole will start to move. The motion will be a combination of thermal velocity plus drift velocity parallel to the direction of the applied field. At lower values of electric field intensity, the drift velocity v is proportional to the magnitude of the field, thus giving a relation:

$$v_e = \mu_e \epsilon, \quad v_h = \mu_h \epsilon, \tag{2.3}$$

where μ is a mobility for electrons or holes and ϵ is the electric field magnitude. In semicondutors, the mobility of both charge carriers is approximately the same. For higher electric field values, the velocity rises slowly until it reaches a saturation velocity which does no longer change with increasing intensity. The saturated velocities are of the order of 10^7 cm/s. [1]

Atomic number	14
Atomic weight	28.08
Atoms	$4.99 \cdot 10^{22}$ cm^{-3}
Stable isotope mass numbers	$28 - 29 - 30$
Density (300 K)	2.33 g/cm^3
Dielectric constant	11.7
Forbidden energy gap (300 K)	1.12 eV
Forbidden energy gap (0 K)	1.17 eV
Electron mobility (300 K)	1350 cm^2/(V $\cdot$ s)
Hole mobility (300 K)	480 cm^2/(V $\cdot$ s)
Electron mobility (77 K)	1350 cm^2/(V $\cdot$ s)
Hole mobility (77 K)	480 cm^2/(V $\cdot$ s)
Electron diffusion constant	34.6 cm^2/s
Hole diffusion constant	12.3 cm^2/s
Intrinsic carrier density (300 K)	$1.45 \cdot 10^{10}$ cm^{-3}
Intrinsic resistivity (300 K)	235 kΩcm
Melting point	1415 °C
Thermal expansion coefficient	$2.5 \cdot 10^{-6}$ 1/ °C
Breakdown field	30 V/μm
Energy per electron-hole pair (77 K)	3.76 eV

Table 2.1: The physical properties of silicon. [7, 8]

2.1.1 Types of semiconductors

There are three types of semiconductors which vary in the type of impurities: intrinsic, n-type and p-type. A new variable to better describe properties of semiconductors is introduced:

$$\rho = \frac{AV}{Id} = \frac{1}{en_i(\mu_e + \mu_h)}, \tag{2.4}$$

The resistivity ρ is defined for a semiconductor with thickness d and surface area A through which current I will flow when a voltage V is applied across the thickness. The second part of the equation uses electron charge e, intrinsic carrier density n_i and the mobility of electrons and holes.

In an intrinsic detector the number of electrons in the conduction band is exactly the same as the number of holes in the valence band. This is typically denoted as $n_i = p_i$, where n is the concentration of electrons in the conduction band and p is the concentration of holes in the valence band. The necessary condition shows clearly that it is impossible to produce real intrinsic detectors (due to residual impurities), but they are of theoretical importance. The resistivity for intrinsic silicon at room temperature is $\rho = 2.3 \times 10^5\ \Omega \cdot$ cm. [1]

In an n-type or p-type semiconductor a dopant is added to an intrinsic semiconductor to change its properties. In the case of n-type detector the impurities are called donors. The elements used are usually phosphorus (P) or arsenic (As) from the group V with five valence electrons. The scheme of this process is shown in Fig. 2.1a – the donors contribute extra electrons to the conduction band, thus making the electrons the majority charge carriers and the holes the minority charge carriers. The equilibrium concentration of holes of electrons must be equivalent to the constant given by the intrinsic silicon: $np = n_i p_i$. The resistivity of a n-type detector is given as:

$$\rho = \frac{1}{en\mu_e}, \tag{2.5}$$

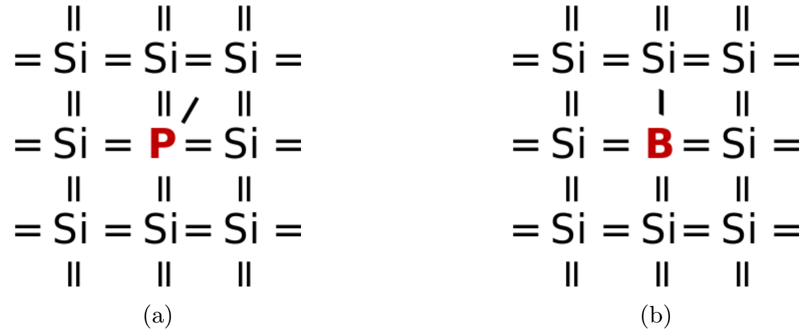

Figure 2.1: Types of impurities in semiconductors: donor impurity (left) and acceptor impurity (right).

For a concentration of electrons $n = 10^{13}/\mathrm{cm}^3$ the resistivity of silicon will be $\rho = 500\Omega \cdot \mathrm{cm}$. [1]

The impurities in a p-type material are called acceptors (scheme in Fig. 2.1b). The elements used in this case are for example boron (B) or aluminium (Al) from group III, which have three valence electrons. In a p-type material, the majority carriers are holes and the minority carriers are electrons.

In case of heavily doped thin layers of semiconductor, a special notation is used: n^+ and p^+ for n-type and p-type semiconductors, respectively.

2.1.2 The p-n junction

The joining of a p-type and n-type crystal together is called a p-n junction. After joining p-type and n-type semiconductors, a diffusive migration of majority carriers across the junction appears. The regions nearby the p–n interface lose their neutrality and become charged, forming a depletion layer (see Fig. 2.2). The barrier created by the migration of charge carriers stops further migration and is called the built-in potential and is of the order of a few hundred milivolts. The depletion zone width can be expanded by applying an external voltage (bias voltage, V_B). The depletion zone width, W, is given as: $W = \sqrt{2\varepsilon\rho\mu V_B}$, where ε is the dielectric constant, ρ is the material resistivity and μ is the majority carrier mobility. The best signal-to-noise ratio is reached in fully depleted detectors. The background in a detector created with p-n junction is caused by the thermally generated minority charge carriers. Under equilibrium conditions (no external forces such as voltages, electrical fields, magnetic fields, or temperature gradients are acting on the semiconductor) electron-hole pairs are generated throughout the volume of the detector. Without external voltage these carriers recombine. However, if an electric field is present, the pairs are separated and sent in different directions. This drift gives rise to a so called leakage or reverse current.

2.2 Types of semiconductor detectors

In this section semiconductor detector types other than pixel detectors (which will be thoroughly described in the next section) will be presented. In respect to the character of pixels all three are position-sensitive semiconductor detectors.

Pad detectors

Pad and pixel detectors are often categorised together. The convention has it that if the dimensions of the individual electrodes are of the size of 1 mm or larger, then they are called pad

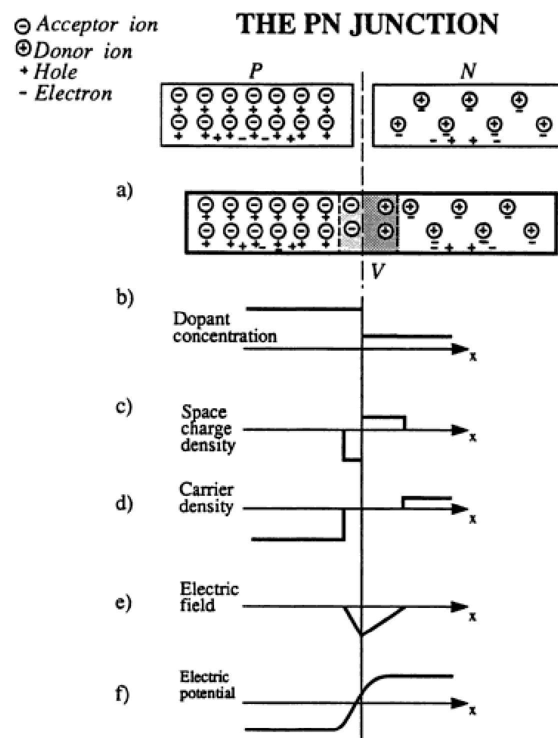

Figure 2.2: The p-n junction. a) Two crystals of opposite type are brought together and a depletion layer is formed on either side of the junction. b) The dopant concentration. c) Net space charge density showing zero charge except for a dipole layer at the junction. d) Electron and hole density through the crystal showing no free carriers in the depleted zone. e) Electric field distribution. f) The potential distribution within the depletion region. [7]

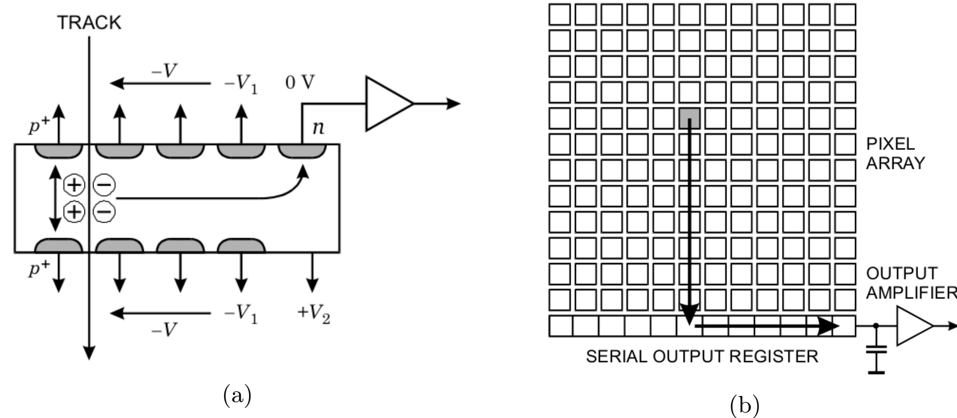

Figure 2.3: Structure of a silicon drift detector (left). Layout of the surface of a CCD (right). [9]

detectors (devices with smaller electrodes are called pixels). In this case, the position readout is simple – the resolution of the detector is given by the width of the pad. To achieve x-y resolution two orthogonal layers of pads are used. The advantage of pads is that the small size reduces the electronic noise and its advantage over pixels is in the electronics processing (in pixel detector every small electrode has its separate readout).

Microstrip detector

Another position sensitive detector similar to pads and pixels is microstrip detector. In this case, the series of narrow parallel strips are fabricated on one surface. The strip width is as small as 10 μm. They are in a n-type block and collect the charges.

Semiconductor drift detectors

These detectors use the drift time of charge carriers to determine the position of incoming particle. As can be seen in scheme in Fig. 2.3a, the n-type bulk is depleted from both surfaces by a series of p^+ electrodes, biased to provide a positive potential gradient along the center axis of the detector. When a particle passes through the depleted area, the holes created drift to the nearest p^+ electrode, whereas the electrons travel to the collection electrode, where the signal is read out. The position is then determined from the time it took the signal charge to drift to the output.

Charged coupled devices

Charged coupled device (CCD) is nowadays most known for its use in digital cameras. The area of a CCD is built from a large number of small pixels (see Fig. 2.3b for a layout), which are connected and read out together. The signal charge deposited in a pixel is then shifted through neighbouring pixels until it reaches an end. The voltage is set so that every pixel has its own potential well to prevent free electrons from liberating. The advantage of CCDs lies in the simplicity of its serial readout technique and also in its ability to distinguish small charge packets.

2.3 Pixel Detectors

Pixel detectors are small volume semiconductor detectors capable of high granularity in detection provided by the pixel size. They are capable of good time and space position recognition. Fig. 2.4 shows a typical pixel cell, a building block of a hybrid pixel detector. The word hybrid denotes

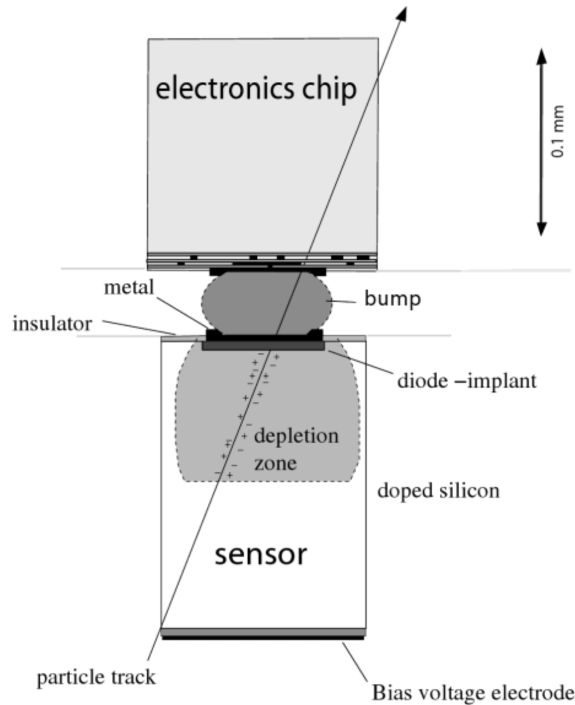

Figure 2.4: Schematic view of one pixel cell. [10]

that the sensor and electronics are fabricated separately and then assembled together via the so called bump bonding. The ionizing particle crosses a sensor, generating charges along the way that are drifted to the diode where they produce signals. These are then amplified and stored by the electronics.

Other from hybrid pixel detectors, there are also monolithic pixel detectors; meaning that the detector and readout electronics are integrated in a monolithic structure. However, this method has its drawbacks, such as the basic incompability between the high-resistivity silicon needed for substantial depletion region for the detector and the lower resistivity silicon used in fabrication of integrated circuits. Next, the detector needs low temperature and high voltage for proper functioning, whereas the integrated circuits undergo high-temperature processes and feature lower voltage characteristic. [1]

In this work only silicon pixel detectors are mentioned, however pixels are also made from other materials, such as Ge, CdTe, or SiC. The choice of a material depends on the field of application, detector efficiency and sensitivity or other detector properties.

These detectors are currently widely used in high energy physics (HEP) experiments. For this application, they have to not only have excellent space and time resolution, but also be radiation hard and do basic triggering (i.e. memorize hit patterns and extract the interesting hits).

2.3.1 Processing

The fabrication technology of silicon detectors is derived from the planar technology which is described hereafter. The cross-section of a particle detector is shown in Fig. 2.5. The individual stages of processing are shown in Fig. 2.6. In this case the outcome will be a p^+-n-n^+ detector, however p^+-i-n are also fabricated (see Section 2.6 in Ref. [10] for their processing).

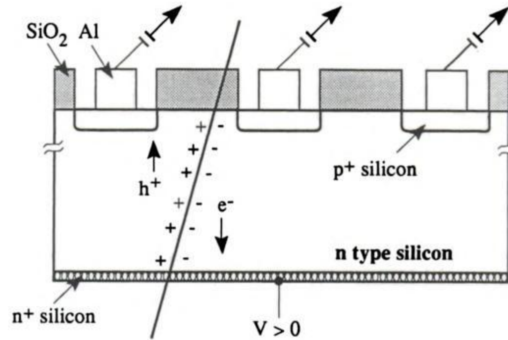

Figure 2.5: Cross-section of a silicon particle detector. [7]

The first step is the thermal oxide passivation of the silicon wafers which serves to protect the wafer surface with a thin layer of SiO_2. The thin layer is achieved by storing the wafer at a temperature between 900 and 1200 °C in an oxygen atmosphere. Next, windows need to be open in the oxide to enable the ion implantation in the desired areas. This is achieved through litographic and etching techniques. The photolitographic masks are used to create a 'hole' in the wafer and then etching is used to copy the structure of photoresist into the underlaying layers. The next step, doping, is done either by implantation (shown in the aforementioned figure) or by diffusion. Fig. 2.6 shows typical values of ions energies and densities in implantation. The advantage of this process is its reproducibility – the implantation dose can be precisely measured. Also, since this process is performed at room temperatures, the photoresist mask can be used to mark the areas not to be doped. Diffusion, on the other hand, is affected by the gradient of the concentration: most dopant can be found at the surface. The dopants enter the wafer at a temperature of 800 to 1200 °C. This temperature is too high for the photoresist, thus the wafer has to be protected with an oxide layer. Next step is annealing which serves to reduce the damage caused by the irradiation with the heavy ions and to diffuse the dopants further from the surface.

The doped wafers are then metallized to provide a low resistivity connection because bonding is possible only on metals. A typical thickness is 1 μm. The surface of the wafer is then covered with aluminium and the desired pattern is achieved with passivation. The wafer is then ready for cutting.

2.3.2 Pixels at ATLAS detector

The first step in the history of the hybrid pixel detectors were taken in 1984 during the IEEE Nuclear Science Symposium, where a note was presented by Gaalema [12] showing the potential hybridization of detectors via bump-bonding and the concept of a circuit in each pixel. This sparked interest at CERN, a high energy physics laboratory located at the Franco-Swiss border, and a study was performed, whose result was the first pixel circuit with signal processing functions and a binary output. The results of measurement of this chip were presented in 1989. The RD19 collaboration (the LHC detector development collaboration) was interested in pixel detectors because of their capability to handle high multiplicity, which had been expected at LHC. Thus in 1994, with collaboration of heavy-ion experiment WA97, first pixels were used to collect data. The Delphi experiment for the Large Electron-Positron collider (LEP) practically separated from the RD19 collaboration and developed their own pixel detectors for Vertex Forward Tracker. These detectors were installed in 1997. Further description of the beginnings of the pixel detectors can be found in Ref. [13].

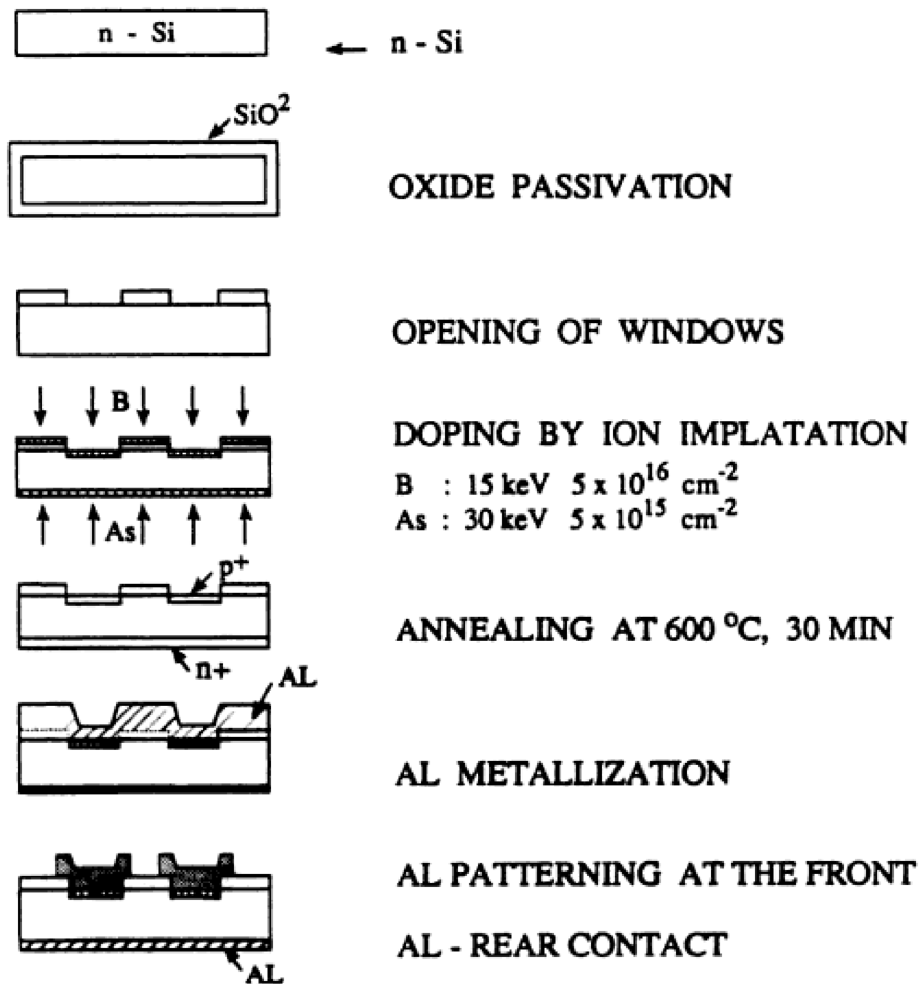

Figure 2.6: The planar process for detector fabrication. The dimensions are not to scale. [7]

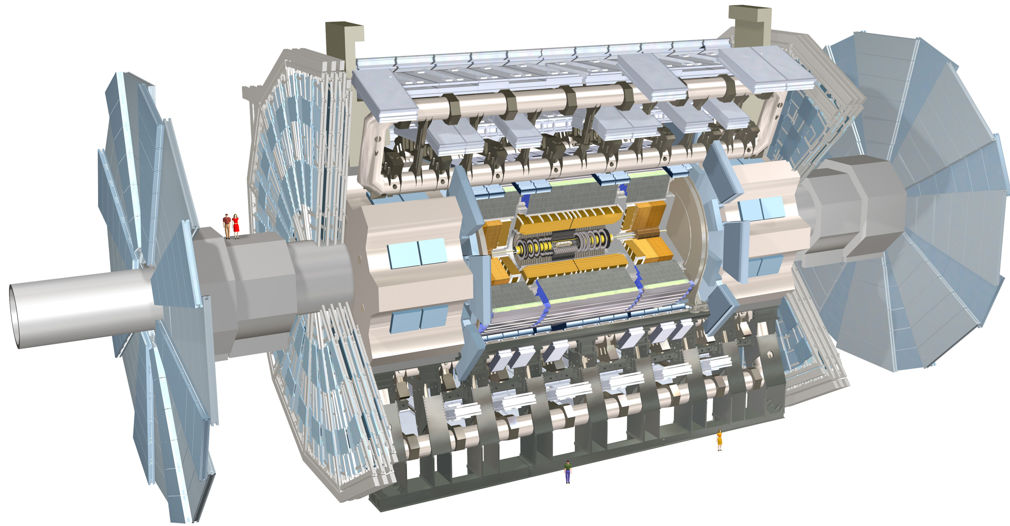

Figure 2.7: The ATLAS detector. [11]

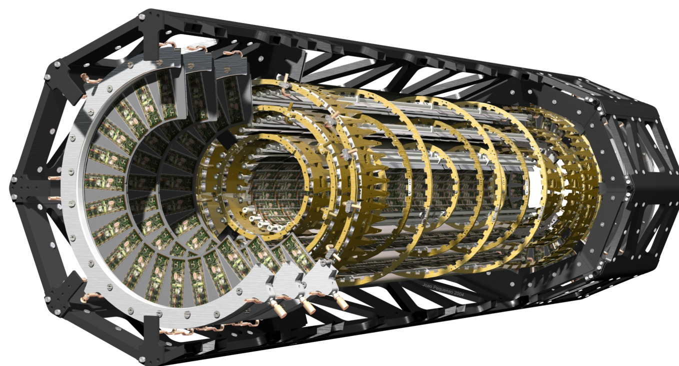

Figure 2.8: The ATLAS Pixel detector. [11]

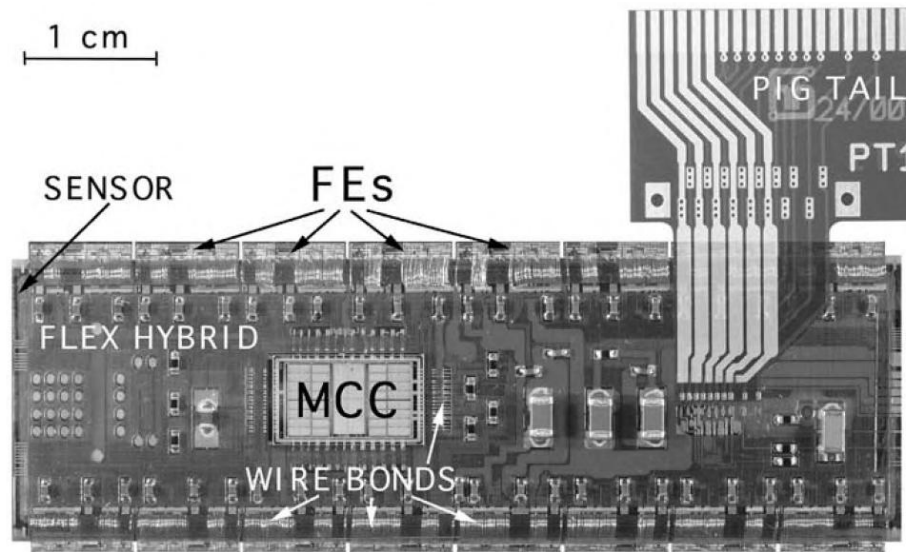

Figure 2.9: The ATLAS Pixel module. [10]

Pixel detectors are currently used in the innermost layer of the ATLAS detector, part of the Large Hadron Collider (LHC) located in CERN. The aim of the ATLAS is to analyze all particle tracks coming from a collision of two protons (or, in some cases two nuclei). This is achieved through an elaborate set of detectors.

The name ATLAS stands for A Toroidal Large ApparatuS with a length of 45 m and 25 m in diameter[1]. Closest to the interaction point is a barrel consisting of pixels (for a scheme of ATLAS see Fig. 2.7 and for a closeup of the pixel part see Fig. 2.8). It consists of three layers of radii 5.0, 9.8, and 12.2 cm that are built with 22, 38, and 52 staves respectively. The three barrel layers are made of identical staves inclined with azimuthal angle of 20 degrees. Stave is a building block composed of 13 pixels.

In the pixel module (shown in Fig. 2.9) there are 16 front-end (FE) chips and one Module Control Chip (MCC). The FE chips are connected through bump bonding to the sensor. Each chip consists of 2880 pixel covering an active area of $0.74 \times 1.09\ cm^2$. The MCC serves to connect the front-end chips to the readout system. It has a 45 kbit storage memory dedicated to the event building at the module level. The MCC receives external data and sends its data out through optical fibers. The time resolution of the chips is below 25 ns to satisfy the expected value of luminosity at LHC.

In conclusion, all modules used are equal to simplify the manufacturing process. The sensors are built using n-doped silicon with n^+-pixel implants.

[1]As the promotional materials like to point out, this is more than 8 store high building.

3 Medipix

One of the pixel detectors currently in use is a Medipix chip (and its succesor, Timepix chip). This chapter serves as an introductory text for these chips. Both of the chips were developed within the context of the Medipix2 collaboration. This collaboration was founded in 1999 with the aim of integrating the pixel technology into different fields other than high energy physics (HEP). It consists of 17 member institutes all around the world. The Medipix2 chip was ordered into production in 2002. In 2005 the arrival time information was requested from the EUDet Consortium, which resulted into the development of the Timepix chip. This chip was ordered into production starting 2006 when an engineering run was launched.

3.1 Medipix2

The Medipix2 chip consists of 256×256 identical elements. Each pixel cell contains around 500 transistors and its size is 55 μm $\times$ 55 μm. A 20 μm in a diameter octagonal opening connects the detector and the preamplifier input via bump-bonding. The chip is constructed so that the non-sensitive area is minimized – the periphery is placed on the bottom of the chip. The periphery contains 13 8-bit DACs and the Input/Output control logic. Both the analog and digital circuitry have been designed to operate with independent 2.2 V power supplies with a total analog power consumption of about 500 mW. The chip contains around 33 million transistors.

A schematics of the Medipix pixell cell is shown in Fig. 3.1a. Each pixel has eight independent configuration bits. Six of them are used for the fine threshold adjustment (three bits for each discriminator), one for masking noisy pixels, and one to enable the input charge test through the 8 fF on-pixel capacitance. The analog side contains a charge preamplifier with DC leakage current compensation, a test capacitance, and two branches of identical discriminators. The digital side contains the Double Discriminator Logic (DDL) and the 13-bit shift register. The front-end can be programmed to be sensitive to either electrons or holes. [14]

The created charge enters the pixel and the amplified voltage is compared with two thresholds. The threshold values are set by two 10-bit DACs on the periphery and can be adjusted by 3-bit thresholds on every cell to reduce pixel-to-pixel noise ratio. If the voltage falls in the range of the threshold then a single pulse is generated at the output of the double discriminator logic. An external shutter signal is applied to the chip. When the shutter is active, the pulses from the double discriminator logic are connected to the clock of the pseudo-random counter within the pixel, each pulse generating one increment. When the shutter is low, the counter becomes a shift register and the pixels in one column are connected together as one long shift register for readout. The chip readout can be performed using a single LVDS driver within 5 ms at a readout clock frequency of 200 MHz or using a 32-bit CMOS bus within 300 μs using a 100 MHz clock. The minimum signal which can be detected on all pixels is ~ 900 e^-. [15]

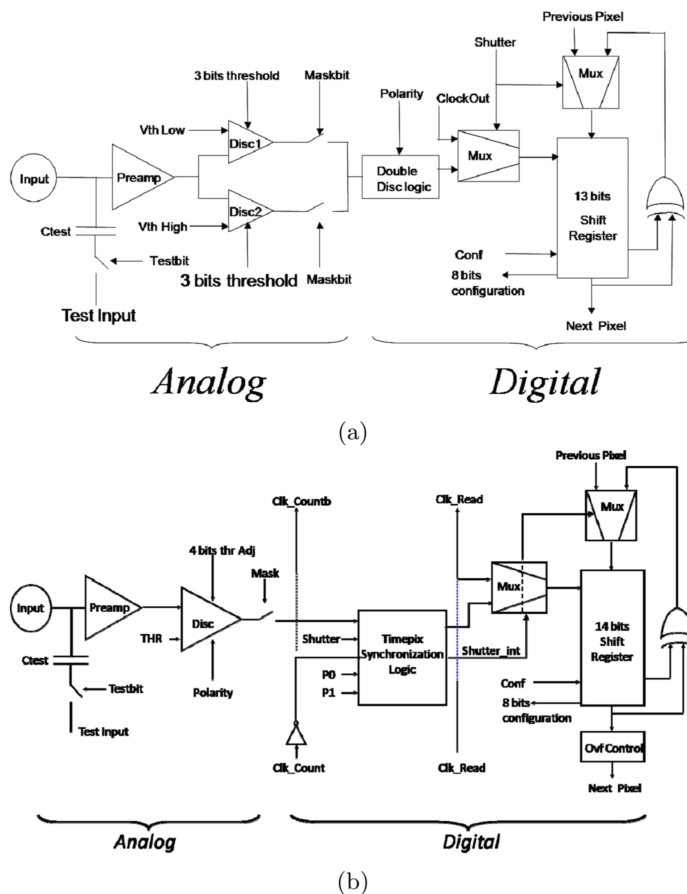

Figure 3.1: Schematic diagram of (a) the Medipix2 and (b) the Timepix pixell cell. [15]

3.2 Timepix

The Timepix chip is a modified version of the Medipix2 chip, which allows for measurement of the arrival time,"time-over-threshold" (TOT) and/or the event counting independently in each pixel. An external reference clock is used to generate the clock in each pixel that increments the counter depending in the selected operation mode. The chip has the same size, readout architecture and floorplan as the Medipix2 chip, thus allowing the use of existing readout systems. [16]

The Timepix pixel cell is shown in Fig. 3.1b. The analog part is very similar to the one of Medipix2 chip; however, only one threshold is available per pixel, but it can be tuned locally with 4 bits. The operating mode of each pixel during data acquisition can be chosen by the user. In the event counting mode, the pixel has the same functionality as Medipix2, the counter being incremented each time the discriminator switches. In the arrival time mode, the counter is incremented by the externally applied clock from the moment the discriminator fires until the shutter is closed. In Time over Threshold mode (ToT), the counter is incremented by the clock as long as the discriminator is active providing information about the total charge deposited in a pixel during the shutter opening time. The minimum signal which can be detected on all pixels is ~ 650 e^-. [15]

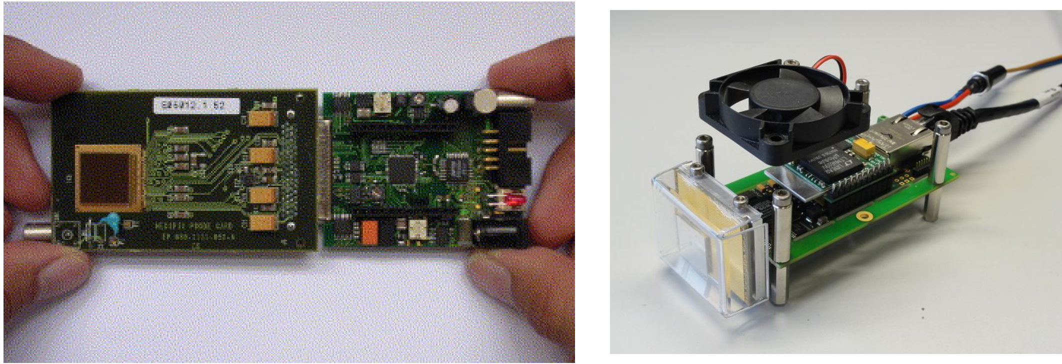

Figure 3.2: Left: picture of the USB interface board ($75 \times 46\text{mm}^2$) connected to the Medipix2 chipboard. [18] Right: RelaxD module; the quad module can be seen at the left part of the figure. [21]

3.3 Readout systems

The first interface board between the Medipix2 chip and a general-purpose commercial PCI-based acquisition card to be used for communication with PC was MUROS2 system [17] developed in Nikhef, Amsterdam in 2003. Next came the USB readout software [18] developed by IEAP CTU in 2006. Other readout systems have been developed by Collaboration members for their own purposes, but are not of importance for this thesis.

The first software readout used with MUROS2 was Medisoft4 [19] developed by the group in Naples. In 2006, the IEAP CTU group developed another software readout both for MUROS2 and USB readout called Pixelman [20]. The Nikhef group in cooperation with IOP ASCR developed a RelaxD system [21, 22].

MUROS2

The NIKHEF group developed a MUROS1 system for the Medipix2 predecessor, the Medipix1 chip. Since it became a standard in most characterization and application uses, when the new chip arose, a new readout system for this chip, MUROS2, was developed. The name MUROS stands for Medipix re-Usable Read Out System. The main component on the board is a FPGA that implements control and data acquisition. Next on the board are clock source, digital transceivers, four Digital-to-Analog-Converters (DACs) and one Analog-to-Digital-Converter (ADC). MUROS2 is capable of acquiring up to ~ 5 frames per second (fps) at 50% duty cycle using a singlechip and about 5.5 fps when reading out a quad assembly[1].

USB interface

The USB interface is using the most widespread PC interface. The standard used is USB 1.1 with the readout speed 6 Mbit/s (6 fps). The USB also provides not only the communication lines but also the power line (5 V, up to 500 mA). One of the advantages of this interface board is that all the detector support is in one compact device ($80 \times 50 \times 20$ mm^3). The interface consists of several blocks. Firstly, the USB interface block is composed of FT245BM chip (the USB info needs to be converted into CMOS logic of the chip). Next components are the block of power supplies and serial line logic converters from LVDS to CMOS logic for communication with the Medipix2 chip. The interface board connected to the Medipix2 chip can be seen in Fig. 3.2 left.

[1] A quad assembly is a 2×2 matrix of connected chips.

RelaxD

RelaxD system consists of a quad readout module (shown in Fig. 3.2 right) and its accompanying readout software RelaxDAQ. The name stands for high-REsolution Large Area X-ray Detector. The module is designed so that it would be possible to 'tile' more than one quad assembly together. The hardware core of the RelaxD module is a FPGA[2], which controls the various devices on the module and the external interfaces (USB, Gigabit Ethernet and the Medipix devices). The USB is used for problem diagnosis during development and the Gigabit Ethernet is the main communication port for control and data flow in both directions. To adjust to differences of reading out the quad modules, special software was developed. The Pixelman software is still used for configuration of the Medipix devices, but a new software called RelaxDAQ is used for fast readout, frame data storage and frame display for up to 4 RelaxD modules.

[2]Field Programmable Gate Array.

4 Radiation hardness

The ionizing radiation makes irreversible changes to the material of the detector called radiation damage. The study of radiation hardness engages in finding the resistivity of the detector to damage or malfunctions caused by ionizing radiation. Radiation causes changes in all parts of the semiconductor detector: sensor as well as electronics. Radiation defects can be divided into two groups, surface and bulk damage. However, this thesis is only concerned with the surface damage of the electronics. Radiation damage to bulk is not significant, since the layer of the oxide is too thin for this damage to manifest. Sensor is not studied, because its fabrication material is not known, thus the radiation effects cannot be properly studied.

Radiation damage creates either point defects and defect clusters. The cluster model was first proposed by Gossick in 1959 [23] in order to explain the very high minority carrier recombination rate observed after irradiation with heavy particles compared to the one observed after gamma or electron irradiation. However, this model is still poorly supported by experimental data, thus not very much is known about the exact nature of the defects. [24] Point defects, on the other hand, are intensely studied and classified into appropriate groups.

There are two main radiation damage mechanisms:

- Displacement damage
- Ionization damage

In the first case, the incident radiation displaces silicon atoms from their lattice sites resulting in a defected crystal with changed electronic characteristics. In the latter case, the absorbed ionization energy liberates charge carriers, which then diffuse or drift to other locations where they are trapped, leading to unintended concentrations of charge. Most systems are sensitive to both these phenomena.

4.1 Displacement damage

Displacement damage is proportional to non-ionizing energy loss. Since energy loss is a process depending on the mass and energy of the incident quanta, the damage must be specified for a specific particle type and energy.

Displacement damage causes formation of mid-gap states, trapping and a change in doping characteristics (donor or acceptor density). The role of mid-gap states is illustrated in Fig. 4.1. Direct transitions between the conduction and valence bands is highly improbable for Si detectors, however, the intermediate states in the forbidden gap provide "stepping stone" for emission and capture process (Fig.4.1a and 4.1b). This easier transition in the depleated region results in an increase in the current. 4.1c and 4.1d show a situation where a defect state captures an electron from the conduction band, which in turn can capture a hole. This process reduces current flowing in the conduction band. [25]

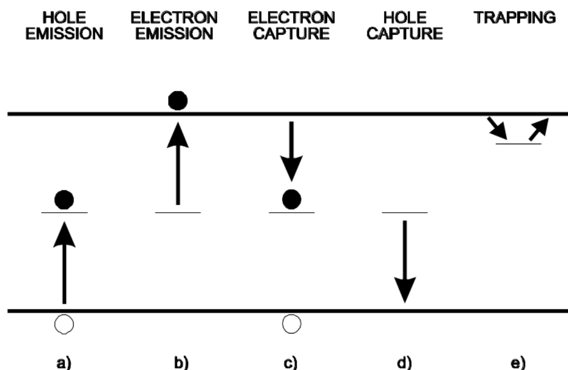

Figure 4.1: Emission and capture processes through intermediate states. [25]

Trapping (Fig. 4.1e) is a process in which states close to the band edges capture a charge and release it after a certain time.

4.2 Ionization damage

Ionization damage is proportional to the absorbed energy, independent of type of radiation. Since the charge liberated depends on the absorber material, the ionizing dose must be referred to a specific absorber, e.g. 1 Gy(Si).

Ionization damage can cause formation of parasitic field. The ionization effects are determined by various attributes: interface trapped charge, the mobility of trapped charge and the time and voltage dependence of charge states. [25]

4.3 Radiation damage in silicon detectors

Radiation damage mechanisms in silicon particle detectors are caused by displacing a primary knock on atom out of its lattice resulting into a so-called Frenkel pair: a silicon interstitial and a left over vacancy. Electrons need kinetic energy of about 255 keV to produce a Frenkel pair and more than 8 MeV to produce a cluster [24]. For the ^{60}Co radiation source used in the measurements the secondary electrons come mainly from the Compton effect with maximum energy of about 1 MeV which is not sufficient to create clusters. Since both interstitials and vacancies are very mobile, a large part of Frenkel pairs recombines at room temperature and no damage remains.

Other radiation damage mechanism contributing to the radiation damage is ionization damage. This damage is caused by holes trapped in the SiO_2 that act as a space charge. However, for silicon particle detectors this mechanism has smaller effect (10^{-3} compared to the neutron of the same energy [26]).

5 | Results

In the last chapter results of the measurement will be presented. The chip used in this measurement was the Timepix chip introduced in the previous chapter. The aim of this measurement was to study the radiation damage effects on the chip.

5.1 Irradiation setup

The chip was irradiated by a ^{60}Co radiation source producing 1.17 and 1.33 MeV photons. Electrons produced in the β-decay of ^{60}Co were shielded by a 1 mm thick aluminium layer. The irradiation lasted of 29 hours. The three-fourths of the chip were covered with 3 lead steps with thickness 2 mm for each step, forming a lead stairway structure allowing us to observe different absorbed doses.

The Timepix chip was read out with Muros 2.1 readout interface. This interface was chosen because of its better stability over the USB interface. Muros was connected to the chip through standard External Ultra SCSI cable, which allows to screen the readout interface from radiation effects. The detector was read out in periodic intervals 30 minute long with exposure time set to 0.3 s.

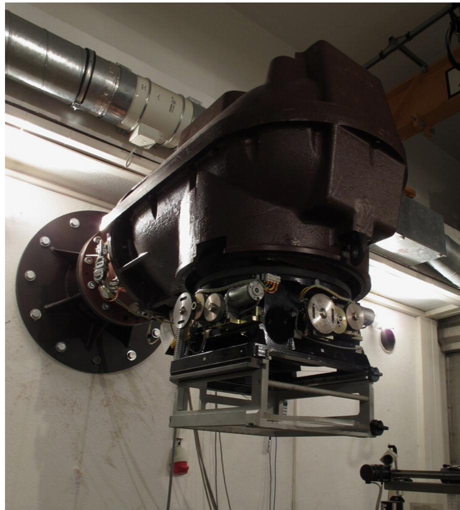

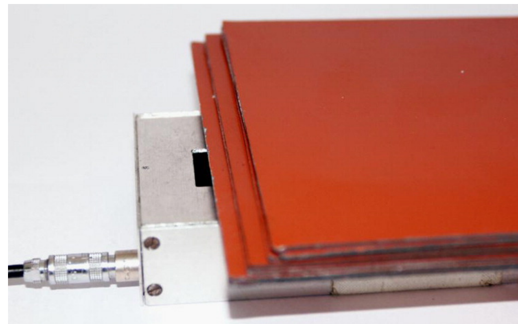

Figure 5.1: ^{60}Co source tube (left) and the lead stairway structure (right). [27]

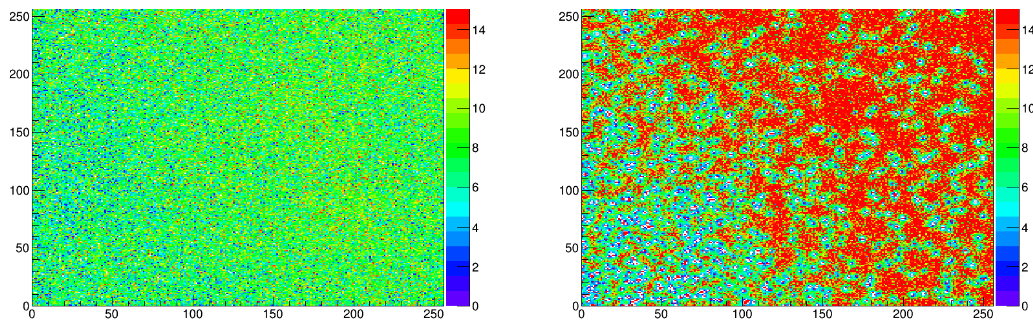

Figure 5.2: Equalization of the chip before (left) and after (right) irradiation.

5.2 Measurement results

Before and after irradiation, an equalization process was performed. Equalization is a process of equalizing individual response of each pixel in the matrix, i.e. each pixel is probed and an individual threshold is set for each pixel. The resulting matrix is shown in Fig. 5.2. The red blobs indicate the burn out of the pixel cells caused by radiation – in order to perform the equalization the chip tried to use all avalailable bits of each cell.

Fig. 5.3 shows different measurement results as a function of time. On the left the total number of hits in sensor versus time is shown. The time axis covers the duration of the measurement and is shown in seconds. The radiation damage done to the chip is clearly visible with the descending tendency of the total number of hits in sensor. There are few areas in the figure. The first gap (around 40 to 60 thousand seconds) was caused by the failure of the readout system. Next comes an area in a 'U' shape, where the start of the system annealing is visible. The following lower section (values around 200 million hits in sensor) was taken when the current source switched off. The figure in the middle shows the mean of hits in pixel versus time. Again, the descending tendency is clearly visible. The penultimate figure shows the root mean square of hits in the pixel chip. It is added to show (with the addition of the previous figure) that the more irradiated the chip is, the more random the readout values become. Plotted in the last figure is the total number of active pixels. Worth noting is that at the end of the measurement out of the original 65 536 active pixels only around 15% remained active to some extent. The deterioration caused by irradiation is yet again clearly visible. Also, the ressurection/annealing of chips that occured, when the ^{60}Co source was turned off, is visible.

Fig. 5.4 shows analog and digital current consumption projected onto the number of hits versus time. The current line is composed of two components: stand-by and maximum current consumption. The current limit was set to 1 A. The stand-by line is not significantly affected by the radiation; however, the maximum current consumption quickly raises with the irradiation time. The resulting question is whether it will return back to normal after annealing or stay elevated. This was studied and the result is that that the current values remain elevated – the irradiated Timepix chip consumes 0.1 A more than before the measurement. The current has undergone four phases during the measuremt as shown in Fig. 5.5. The first phase is data acquisition, second one is data processing and the last two are stand-by.

The last two figures, Fig. 5.6 and 5.7, show an image degradation study. The first set shows the layout of the pixel hits and gives visual representation of how each pixel was affected and burn out throughout the radiation. The second set are histograms showing the corresponding pixel hit

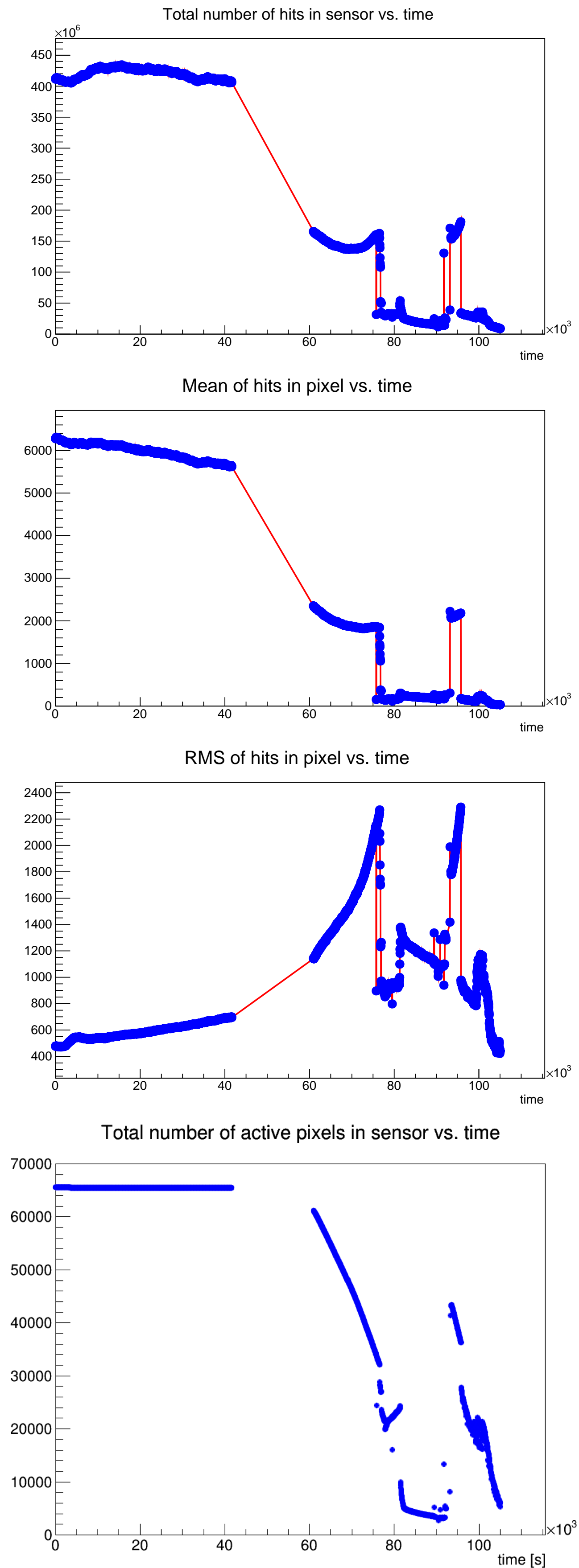

Figure 5.3: The statistical results obtained from the measurement. Further described in the text.

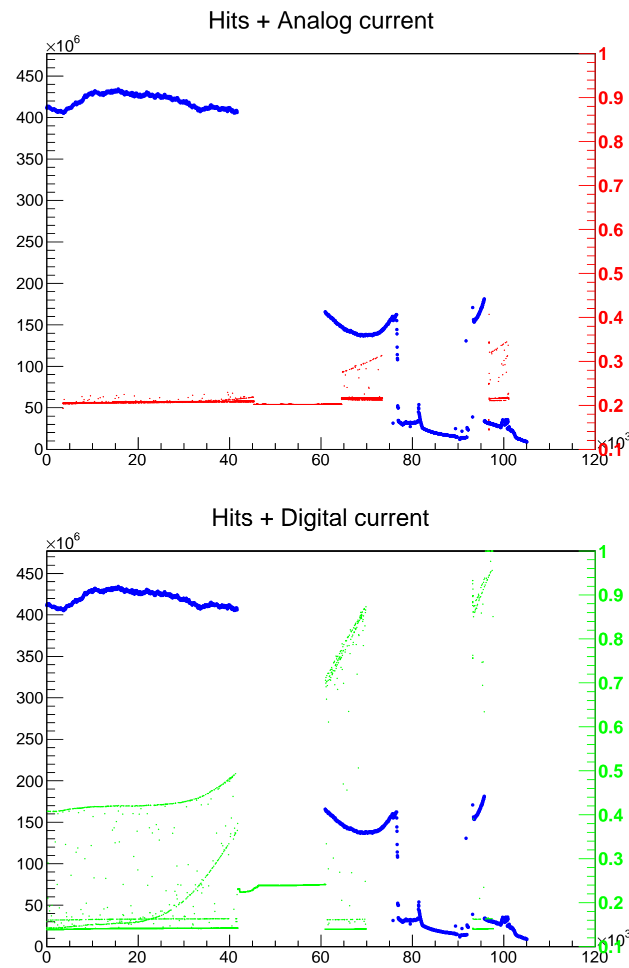

Figure 5.4: Analog (up) and digital (down) current consumption projected onto the number of hits versus time.

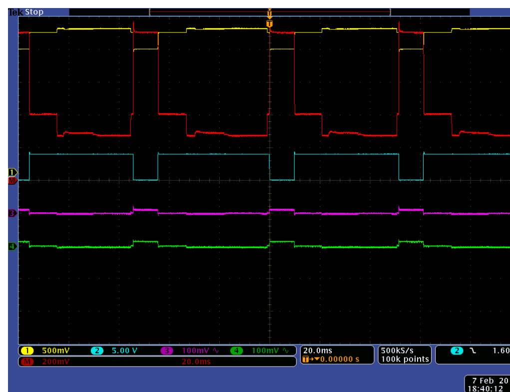

Figure 5.5: The waveform of the four phases of current consumption.

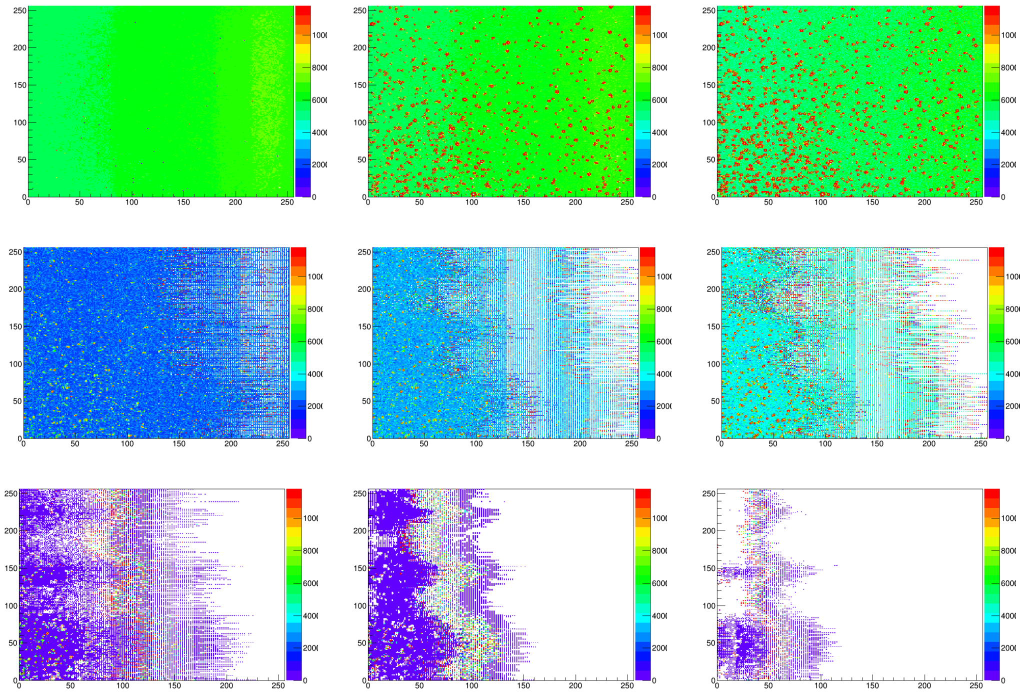

Figure 5.6: Image degradation study. The pixel matrix hit counts are displayed.

count.

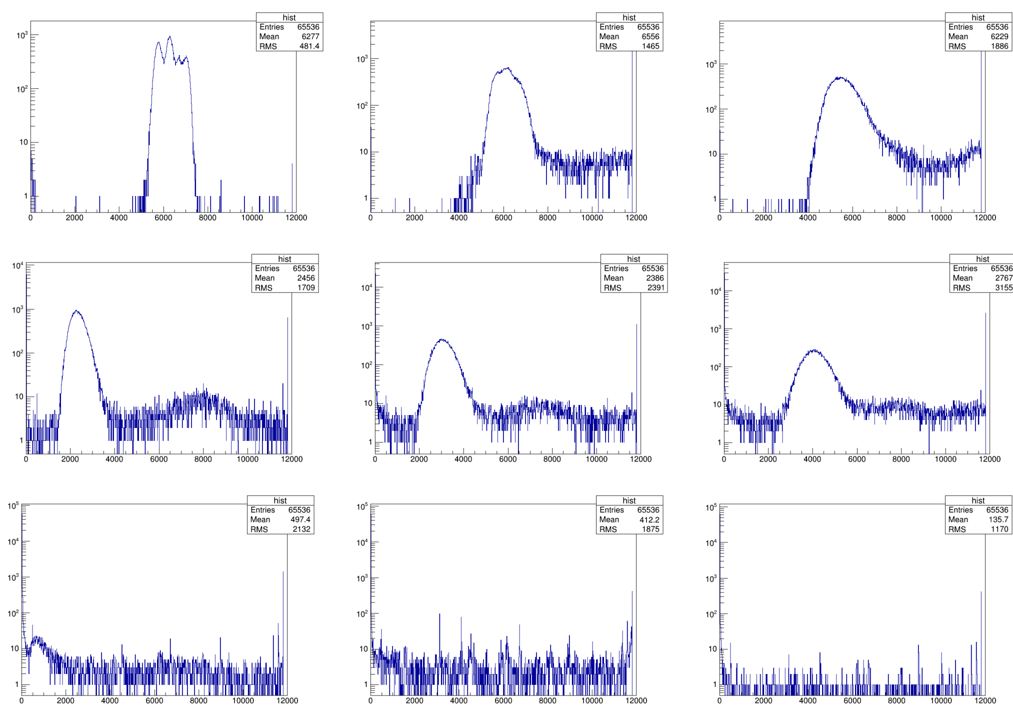

Figure 5.7: Image degradation study. The pixel matrix hit counts histograms are displayed.

Conclusions

The first chapter of this work gives a short presentation of the way particles interact with matter. Next, semiconductors and among them pixel detectors were presented. The third chapter introduced the pixel detectors used in the measurement performed for this work and the fourth chapter introduced some radiation damage processes. All these chapters were written to give a proper background and understanding for the last chapter, that presents the results of a measurement performed with Timepix detector concerning radiation hardness.

While studying radiation damage, the degradation of the Timepix chip was studied. The technology used for the fabrication of this chip was 0.25 μm IBM radiation hard technology with 4 nm thick oxide. It was shown that with increasing irradiation time, the number of hits in the sensor diminished, even though the high-flux γ-ray source was uniformly delivering the ionizing radiation. The burnout performed by the radiation is also visible when comparing the results of an equalization process before and after irradiation.

Both the analog and digital current consumption steadily rose throughout the irradiation. After annealing, the default analog current value of the irradiated Medipix2 chip increased for 0.1 A.

The image degradation study showing how the individual pixel cells degraded was also performed.

Bibliography

[1] G. F. Knoll, *Radiation detection and measurement; 4th ed.* New York, NY: Wiley, 2010.

[2] K. Nakamura *et al.*, "Review of Particle Physics," *Journal of Physics G*, 2010.

[3] "Wolfram Mathematica9 reference center." `http://reference.wolfram.com/mathematica/ref/LandauDistribution.html`, 2013.

[4] "Wikipedia commons." `http://commons.wikimedia.org/wiki/`, 2013.

[5] J. H. Hubbell, H. A. Gimm, and I. Overbo, "Pair, triplet, and total atomic cross sections (and mass attenuation coefficients) for 1 Mev-100 Gev photons in elements Z=1 to 100," *Journal of Physical and Chemical Reference Data*, vol. 9, no. 4, pp. 1023–1148, 1980.

[6] J. Vacík, "Neutron physics." University Lecture, March 25 2013.

[7] A. Peisert, "Silicon microstrip detectors," in *Instrumentation in High Energy Physics*, ch. 1, pp. 1–79, 1992.

[8] G. Bertolini and A. Coche, *Semiconductor detectors.* Amsterdam : North-Holland, 1968.

[9] H. Spieler, *Semiconductor Detector Systems.* Oxford scholarship online, OUP Oxford, 2005.

[10] L. Rossi, *Pixel Detectors: From Fundamentals to Applications.* Particle Acceleration and Detection, Springer, 2006.

[11] The ATLAS collaboration, "Atlas experiment public pages." `http://atlas.ch`, 2013.

[12] S. Gaalema, "Low noise random-access readout technique for large pin detector arrays," *Nuclear Science, IEEE Transactions on*, vol. 32, no. 1, pp. 417–418, 1985.

[13] E. H. Heijne

[14] X. Llopart, M. Campbell, D. San Segundo, E. Pernigotti, and R. Dinapoli, "Medipix2, a 64k pixel read out chip with 55 μm square elements working in single photon counting mode," in *Nuclear Science Symposium Conference Record, 2001 IEEE*, vol. 3, pp. 1484–1488 vol.3, 2001.

[15] M. Campbell, "10 years of the Medipix2 Collaboration," *Nuclear Instruments and Methods in Physics Research Section A: Accelerators, Spectrometers, Detectors and Associated Equipment*, vol. 633, Supplement 1, no. 0, pp. S1 – S10, 2011. 11th International Workshop on Radiation Imaging Detectors (IWORID).

[16] X. Llopart, R. Ballabriga, M. Campbell, L. Tlustos, and W. Wong, "Timepix, a 65k programmable pixel readout chip for arrival time, energy and/or photon counting measurements," *Nucl. Instrum. Methods Phys. Res., A*, vol. 581, no. 1-2, pp. 485–494. 10 p, 2008.

[17] D. S. S. Bello, M. van Beuzekom, P. Jansweijer, H. Verkooijen, and J. Visschers, "An interface board for the control and data acquisition of the Medipix2 chip," *Nuclear Instruments and Methods in Physics Research Section A: Accelerators, Spectrometers, Detectors and Associated Equipment*, vol. 509, no. 1–3, pp. 164 – 170, 2003.

[18] Z. Vykydal, J. Jakubek, and S. Pospisil, "USB interface for Medipix2 pixel device enabling energy and position-sensitive detection of heavy charged particles," *Nuclear Instruments and Methods in Physics Research Section A: Accelerators, Spectrometers, Detectors and Associated Equipment*, vol. 563, no. 1, pp. 112 – 115, 2006.

[19] M. Conti, M. Maiorino, G. Mettivier, M. C. Montesi, and P. Russo, "Preliminary test of Medisoft 4: control software for the Medipix2 readout chip," *Nuclear Science, IEEE Transactions on*, vol. 50, no. 4, pp. 869–877, 2003.

[20] T. Holy, J. Jakubek, S. Pospisil, J. Uher, D. Vavrik, and Z. Vykydal, "Data acquisition and processing software package for Medipix2," *Nuclear Instruments and Methods in Physics Research Section A: Accelerators, Spectrometers, Detectors and Associated Equipment*, vol. 563, no. 1, pp. 254 – 258, 2006.

[21] "Relaxd system." `https://www.nikhef.nl/en/for-nikhef-users/departments/detector-rd/developments/solid-state-detectors/relaxd-system/`, 2013.

[22] V. van Beveren, H. Boterenbrood, and M. Hejtmánek, *Relaxd module: User Instructions & Software Manual*. Nikhef Amsterdam, 2011.

[23] B. Gossick, "Disordered regions in semiconductors bombarded by fast neutrons," *Journal of Applied Physics*, vol. 30, no. 8, pp. 1214–1218, 1959.

[24] M. Moll, "Radiation damage in silicon particle detectors – microscopic defects and macroscopic properties –," Master's thesis, Universität Hamburg.

[25] H. Spieler, "Introduction to radiation-resistant semiconductor devices and circuits," in *AIP Conference Proceedings*, vol. 390, p. 23, 1997.

[26] J. Schwank, M. Shaneyfelt, D. Fleetwood, J. Felix, P. Dodd, P. Paillet, and V. Ferlet-Cavrois, "Radiation effects in MOS oxides," *Nuclear Science, IEEE Transactions on*, vol. 55, no. 4, pp. 1833–1853, 2008.

[27] M. Čarná, K. Dučevová, M. Hejtmánek, O. Konček, and M. Marčišovský, "Evaluation of the Timepix chip radiation hardness using a ^{60}Co source," *Nuclear Instruments and Methods in Physics Research Section A: Accelerators, Spectrometers, Detectors and Associated Equipment*, no. 0, pp. –, 2013.